ERF2011_154

Performance Analysis of a Lightweight Helicopter Featuring a Two–Bladed Gimballed Rotor

Giulio Avanzini*
Università del Salento, Brindisi, 72100, Italy
Guido De Matteis†
"Sapienza" Università di Roma, Rome, 00184, Italy
Federica F. Lucertini‡
"Sapienza" Università di Roma, Rome, 00184, Italy
and
Alberto Torasso§
Politecnico di Torino, Turin, 10129, Italy

Abstract

This paper deals with the investigation of performance and stability characteristics of a two-seater, two-bladed, lightweight helicopter developed in the framework of VLR certification specifications. The main rotor features a gimballed hub with elastomeric bearings equipped with a Bell-Hiller bar to improve stability, while the fixed pitch, rpm controlled, five-bladed tail rotor is a fenestron design.

The main technical drivers of the novel design are to reduce the high level of 2/rev vibrations occurring in teetering rotors, to retain adequate control power in low–g maneuvering and to improve handling qualities using the stabilizing bar to increase roll and pitch damping. A specific aspect of the gimballed rotor is the presence of a sustained wobbling motion of the hub, even in steady–state conditions.

A nonlinear model of the vehicle is developed that includes, among other aspects, a detailed model of main rotor, nonlinear, quasi–static blade aerodynamics, inflow dynamics, a simple fuselage aerodynamic model and a tail rotor model derived from experimental wind–tunnel tests.

Periodic trim conditions are evaluated using a shooting method in order to assess the impact of rotor wobbling motion on helicopter steady–states. Results on performance and controllability are presented and discussed. Finally, the stability characteristics are assessed in order to gain some preliminary insight on the handling qualities of the helicopter.

*Professor, Faculty of Industrial Engineering, Edificio 14 Cittadella della Ricerca, S.S. 7 Km.7.3, e-mail: *giulio.avanzini@unisalento.it*, tel. +39 0831 507427, fax +39 0831 507327; AIAA Senior Member.

†Professor, Department of Mechanical and Aerospace Engineering, Via Eudossiana 18, e–mail: *dematteis@dma.ing.uniroma1.it*, tel. +39 06 44585210, fax +39 06 4881759; AIAA Senior Member.

‡Ph. D., Department of Mechanical and Aerospace Engineering, Via Eudossiana 18, e–mail: *federica.lucertini@uniroma1.it*.

§Ph. D. Student, Department of Aerospace Engineering, C.so Duca degli Abruzzi 24, e–mail: *alberto.torasso@polito.it*, tel. +39 011 5646871, fax +39 011 5646899; AIAA Member.

Nomenclature

C_L, C_D	lift and drag coefficients
$\boldsymbol{DP}$	monodromy matrix
h	flight altitude
K_H	fly–bar/swash–plate command ratio
L, D	lift and drag forces
M	Mach number
n	rotor rpm
$\boldsymbol{p}_I = [N\ E\ D]^T$	position vector in the Earth frame
P	available power
T	rotor thrust force
$\boldsymbol{v} = [u\ v\ w]^T$	velocity vector in body–axes
V	flight speed modulus
$\boldsymbol{x}_B$	rigid–body (fuselage) state vector
Greek symbols	
α, β	angle of attack and sideslip angle
θ_0	collective pitch command
θ_{bl}	blade section pitch angle
θ_{fb}	secondary cyclic pitch command
θ_{cyc}	primary cyclic pitch command
θ_H	rotor longitudinal tilt
θ_{SW}	longitudinal cyclic pitch command
θ_{tw}	twist angle of blade section
λ	eigenvalue
Λ	eigenvalue of the monodromy matrix
μ	advance ratio
$\boldsymbol{\nu} = [\nu_0\ \nu_s\ \nu_c]^T$	state vector of the inflow model
ρ	air density
τ	period of rotor revolution
ϕ_H	rotor lateral tilt
ϕ_{SW}	lateral cyclic pitch command
$\boldsymbol{\Phi} = [\phi\ \theta\ \psi]^T$	Euler angles vector
ψ	blade anomaly

ω	turn rate
$\boldsymbol{\omega} = [p\ q\ r]^T$	angular velocity vector
Ω	rotor rate
Subscripts	
bl	blade
fb	fly-bar
h	horizontal tail
TR	tail rotor
v	vertical fin

Introduction

This paper aims to analyze performance and stability of a novel two–seater, two–bladed lightweight helicopter (dubbed KA–2H and shown in Fig. 1) developed by K4A S.r.l. in the framework of very light rotorcraft (VLR) certification specifications. Among other innovative features for VLRs such as the two-engine configuration and the fenestron, five–bladed tail rotor with fixed pitch blades and variable rpm, the helicopter features a two–bladed gimballed main rotor equipped with a Bell–Hiller fly–bar to improve the damping of rotational motions [1].

More in detail, a rigid yoke is connected to the shaft through a homokinetic spherical joint, realized by means of a set of elastomeric springs (Fig. 2). The blades are connected to the yoke by means of coning hinges, in order to provide a gust–alleviation effect. The impact of coning motion on helicopter performance and response to controls is marginal and coning dynamics is thus neglected in the derivation of the model. A fixed coning angle $\beta_1 = \beta_2 = 1.8$ deg is assumed in the sequel.

The rotor yoke thus features two mechanical degrees of freedom, that is, rotations around the teetering and feathering axes. The feathering motion is coupled with blade pitch command and it is driven by the fly–bar, which features two low aspect ratio paddles at the tips. Finally the hub has some undersling to limit 2/rev loads.

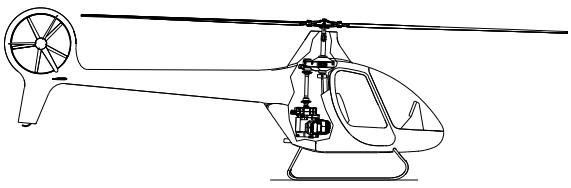

Figure 1: KA–2H helicopter.

The rotor hub is designed with the main objective of addressing some of the negative characteristics that affect the dynamics of helicopters equipped with teetering rotors as, for instance, high 2/rev oscillatory loads, poor response characteristics at low gs and a somewhat pronounced sensitivity to gusts and/or large pilot inputs.

The analysis of the gimballed hub [1,2] shows that in most flight conditions a wobble (precession) motion develops, that is, the hub axis, orthogonal to the plane defined by the blades axis and the fly-bar axis, describes a cone about its mean position at twice the rotor rotational frequency even in steady–state conditions. This unusual rotor behaviour can affect considerably helicopter performance in terms of - among others - controllability and handling qualities which deserves a detailed analysis of (periodic) steady–states and their stability.

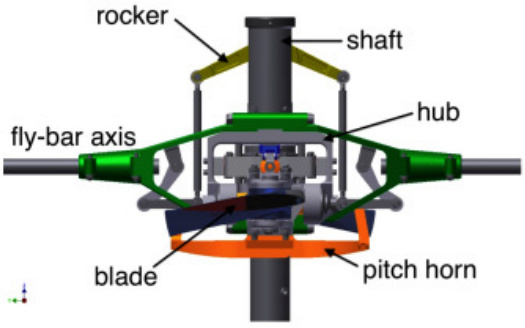

Figure 2: Main rotor hub.

In order to investigate trim conditions in a wide portion of the expected operating flight envelope, non-linear rotor and fuselage models are developed and analyzed, with the main objectives of supporting the design phase of the helicopter. In particular, an estimate of reasonable performance limits and a preliminary handling quality assessment are performed on the basis of a complete aerodynamic helicopter model. Together with other minor effects, a constant rotor rpm is assumed in the derivation of the model, thus neglecting engine dynamics, a reasonable assumption within a study focused on steady–state performance.

Two different trim techniques are used, in the framework of performance and controllability analysis, on one side, and stability analysis on the other one. In the first case, a periodic shooting method [3,4] for the complete helicopter model with fully coupled fuselage, rotor and inflow dynamics is devised. A nested trim technique is adopted for the stability analysis [5], where periodic steady states are evaluated for a decoupled rotor model (featuring rotor mechanical degrees of freedom and inflow states only), whereas fuselage degrees of freedom are trimmed on the basis of average rotor loads. This second technique allows for a more straightforward derivation of helicopter stability derivatives, required to carry out the stability analysis through the linearization of the rigid body model of the rotorcraft. In this case, a quasi–static rotor response is assumed.

A stability analysis for the complete model of the vehicle (rotor, inflow and fuselage) is carried out by application of a Poincaré map methodology, in order to validate the results obtained on the basis of the quasi–static model. At the same time, the physical interpretation of the eigenstructure of the linearized helicopter model allows for a better understanding of the results of the Poincaré analysis, obtained in terms of eigenvalues for a discrete map.

These eigenvalues are used for a preliminary evaluation of handling qualities against stability requirements obtained from CS-27 specifications.

In what follows, the main features of the rotorcraft model are illustrated in the next section. Then, in the third section, the methodologies for trim analysis are recalled and the vehicle performance characteristics are discussed. The stability analysis is dealt with in the fourth section. A section of conclusions ends the paper.

Rotorcraft Model

Rotor configuration

The rotor configuration is rather unusual and only a very limited number of previous studies is available on the dynamic characteristics of two–bladed gimballed rotors [6,7]. The homokinetic joint is designed to rotate about its axis with the same angular speed Ω of the shaft, even when they are not aligned. In the absence of an engine dynamic model (not necessary in the evaluation of steady–state vehicle performance), a constant angular speed can be assumed, $\dot{\psi}_H = \Omega = \text{const}$.

Inertial and aerodynamic forces developed by the rotor are transmitted to the fuselage through the homokinetic joint. The relative motion between rotor elements (blades, yoke, and shaft) also develops i) elastic moments and ii) elastic and/or friction moments around the blade pitch axis due to the feathering motion, all perpendicular to the hub axis. Finally, the engine torque Q_{eng} is assumed directed along the hub axis.

The governing equations for the main rotor are derived using a Lagrangian approach and, in order to accurately represent the inertial loads, all nonlinear terms are retained in the formulation. A symbolic manipulator software is used to formulate the dynamical model of the rotor. A detailed description of the model can be found in [1].

The assumptions of rigid blades, rigid shaft, constant coning angle and quasi-steady aerodynamics provide a reasonable level of accuracy for the the analysis of rotor behavior and the assessment of helicopter performance.

Rotor aerodynamics

Each blade section is modeled as a two-dimensional airfoil. The wake–induced velocity, that modifies the angle of attack of the blade sections, is provided by the Pitt-Peters dynamic inflow model [8] with triangular distribution on the rotor disk. Stall and compressibility effects are taken into account in the aerodynamic model of the blade airfoil where lift and drag coefficients are expressed in tabular form as functions of angle of attack ($-180 \leq \alpha \leq 180$ deg). A correction for Mach number effects in the range $0 \leq M \leq 0.8$ is also introduced.

Rotor control

The blade pitch command mechanism, shown in Fig. 2, features two contributions:

- a primary command from the swash–plate, represented by a collective blade pitch increment, θ_0, and a cyclic pitch command, $\theta_{cyc} = \theta_{SW}\cos\psi + \phi_{SW}\sin\psi$, where θ_{SW} and ϕ_{SW} are the longitudinal and lateral tilt angles of the swash–plate, respectively;
- a secondary command, that varies the actual value of the cyclic pitch, mechanically driven by hub rotation around the blade feathering axis, θ_{fb}, that corresponds to the flapping of the fly-bar.

Taking into account also the twist angle of the blade section at x along the blade span, $\theta_{tw}(x)$, the local pitch angle with respect to the shaft plane is given by

$$\theta_{bl}(x) = \theta_0 + \theta_{tw}(x) + K_H\theta_{cyc} + (1 - K_H)\theta_{fb}$$

where K_H is the fly–bar/swash–plate command ratio. Note that a secondary command is always present when a teetering rotors features a flybar that is mechanically linked to the pitch horn. As a major difference, the fly–bar is here rigidly connected to the yoke, thus providing a contribution to its dynamic behaviour, the secondary command being determined by the yoke inclination with respect to the shaft axis, as outlined above.

Tail rotor, empennages and fuselage

The tail rotor is a fenestron featuring a fixed pitch shrouded rotor. Thrust control is obtained by varying tail rotor rpm through a hydraulic motor, instead of the usual tail rotor collective pitch command. Tail rotor thrust is expressed by means of a third–order polynomial function depending on rotor speed, n_{TR}, in the form

$$\begin{aligned} T_{TR} &= T_{TR}(n_{TR}, V, \beta_v) \\ &= c_3\, n_{TR}^3 + c_2(V)\, n_{TR}^2 + c_1(V)\, n_{TR} + c_0(V, \beta_v) \end{aligned}$$

where the coefficients c_i, which depend on flight speed V and sideslip angle β_v ($-10 \leq \beta_v \leq 5$ deg), are obtained from least–square approximations of wind tunnel test data.

Horizontal tail and vertical fin are modeled as finite wings. Their lift and drag are given by the classical expressions

$$\begin{aligned} L_{h,v} &= \frac{\rho}{2} V_{h,v}^2 S_{h,v} k_{h,v} C_L(\alpha_{h,v}) \\ D_{h,v} &= \frac{\rho}{2} V_{h,v}^2 S_{h,v} C_D(\alpha_{h,v}) \end{aligned}$$

where $V_{h,v}$ is the wind velocity on the surfaces and $k_{h,v} < 1$ is a factor that depends on the aspect ratio.

The inflow velocity on the tailplane is assumed parallel to the rotor shaft, uniform and constant in the far wake, so that the harmonic components are neglected in the interaction model. Wake radius is assumed constant and equal

to R. No circulation effects are considered. Under these assumptions, the main rotor wake affects the aerodynamic characteristics of the horizontal tail only in an interval of flight velocities, when the airmass accelerated by the rotor impinges on the tail as a result of the combination of vehicle airspeed and inflow velocity increment. The interaction between wake and empennage is modeled using an inflow velocity intensity factor [9,10] for the inflow component normal to the tail surface.

The fuselage aerodynamic model only considers the drag force with the assumptions that the center of pressure is located in the geometric center [11], and the aerodynamic moments due to angular rates are negligible with respect to those developed by tailplane and fin. The drag is

$$D_f = \frac{\rho}{2} V_f^2 S_f$$

where S_f is the equivalent flat plate area, estimated according to [12], and V_f includes the uniform component of the inflow velocity increment [8].

The rotorcraft dynamics is thus described by 19 state variables:

- helicopter fuselage rigid–body states $\boldsymbol{x}_B$: velocity $\boldsymbol{v} = [u\ v\ w]^T$, angular rate $\boldsymbol{\omega} = [p\ q\ r]^T$, Euler angles $\boldsymbol{\Phi} = [\phi_B\ \theta_B\ \psi_B]^T$, c.g. position in the inertial frame $\boldsymbol{p}_I = [N\ E\ D]^T$
- rotor states: tilt angles of the hub $\boldsymbol{\Theta}_H = [\theta_H\ \phi_H]^T$, defined in a non-rotating frame and their derivatives $\dot{\boldsymbol{\Theta}}_H = [\dot{\theta}_H\ \dot{\phi}_H]^T$
- inflow states $\boldsymbol{\nu} = [\nu_0\ \nu_s\ \nu_c]^T$

As a consequence of the aforementioned wobble motion, the rotor states present periodic steady–states in the entire range of flight speed, leading to not negligible periodic loads on the fuselage.

Trim techniques

In what follows, the dynamics of rotor and fuselage will be considered either coupled or uncoupled. In the first case all the state variables (rotor and body) are considered periodic at steady state. In the second approach, only rotor periodic motion is retained, whereas fuselage variables at trim are constant under the action of rotor forces and moments averaged over half a rotation. This is equivalent to a quasi-static assumption [13]. Accordingly, two techniques are used to solve the trim problem for the helicopter.

Periodic trim considers all the state variables, and solves the coupled system (rotor and fuselage) taking into account the oscillations of the fuselage due to the periodic dynamics of the rotor. In particular, trim states are calculated by means of the periodic shooting method [3,4] applied to the complete model of the helicopter (including rotor, inflow and fuselage states). The full set of equilibrium equations is solved using a standard nonlinear algebraic equation solver implementing a Newton–Raphson method. The shooting problem is solved numerically, integrating the equations of motion of the rotor/helicopter with a fourth-order Runge-Kutta algorithm with fixed-step ($\Delta\psi = 2$ deg) from an initial guess.

This technique is adopted for the study of helicopter performance as well as for the stability analysis based on the Poincaré map technique [14].

The nested trim technique in based on uncoupling rotor dynamics from fuselage equations of motion, assuming that the high frequency variations of rotor forces and moments do not affect significantly fuselage variables at steady–state. The structure of the nested trim algorithm consists of two loops: the inner loop identifies a periodic equilibrium condition for the isolated rotor (rotor and inflow states) for the current values of fuselage states and rotor control variables, while the outer loop is a classical trim procedure for the fuselage degrees of freedom, where average rotor force and moment transmitted to the fuselage are determined on the basis of the rotor periodic condition identified by the inner loop. This technique provides an approximate solution of helicopter equilibrium, suitable for the derivation of stability derivatives and the interpretation of the stability characteristics of the vehicle based on the linearization of the quasi–static model.

Helicopter Performance

The periodic trim technique is adopted for the solution of the trim problem for performance analysis. The relevant geometric and inertial characteristics of the vehicle considered in this analysis are reported in Tables 1 and 2 together with some design parameters.

The hub angular position at different values of forward speed in horizontal flight is reported in Fig. 3. The wobbling motion has an amplitude of 1.5 deg in hovering, it reaches a minimum around 35 m/s, and increases up to 2.5 deg at the maximum speed, $V = 60$ m/s. The corresponding values of flapping coefficients of blades and paddles vs. air speed are shown in Fig. 4(a). In hovering, the thrust vector is tilted 2 deg backward to compensate for the forward tilt of the shaft axis with respect to the longitudinal fuselage axis, whereas in forward flight the value of a_{1_s} decreases (thrust vector tilted forward in order to compensate for the pitch–up moment developed by the tailplane.

Note that the moment components delivered to the fuselage are, in part, specific for the gimballed rotor case. Together with the usual moment of thrust developed by tip–path–plane (TPP) rotation, an elastic moment due to the elastomeric joint, proportional to the hub tilt angles with respect to the shaft, and the projection of the in–plane moment along the hub axis are also present. At increasing speed the two latter contributions determines a significant pitch–down moment, as a result of the increasing amplitude of the wobbling motion. This somewhat limits the forward rotation of the TPP.

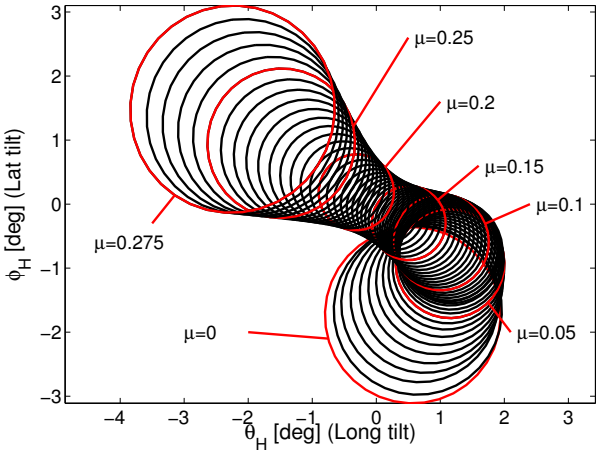

Figure 3: Hub angular position at trim as a function of forward speed.

The lateral flapping b_{1_s} decreases at low speed to compensate for the reduction of the roll moment due to the tail rotor. At higher speed the lateral tilt of the TPP remains close to zero as, again, the forward rotation of the TPP projects a component of the in–plane moment onto the roll axis that balances the moment of the tail rotor.

Figure 4(b) shows the variations of pitch (θ) and roll (ϕ) angles vs. speed, that appear quite conventional. Control angles are reported in Fig. 4(c), where the behavior of collective pitch (θ_0) and tail rotor rpm is also typical for a rotary wing vehicle. As for cyclic pitch, note that, for the considered vehicle configuration, blade pitch depends on two contributions. In particular, at steady–state, when the TPPs of blades and fly–bar are constant [2], θ_{bl} can be written as

$$\theta_{bl} = \theta_0 - A_1 \cos\psi - B_1 \sin\psi$$

with

$$A_1 = K_H \phi_{SW} + (1 - K_H) d_{1s}$$
$$B_1 = -K_H \theta_{SW} - (1 - K_H) c_{1s}$$

where c_{1s} and d_{1s} are fly-bar flapping coefficients, evaluated with respect to a plane perpendicular to the shaft axis (Fig. 4(a)). In spite of the peculiarities of the configuration, the variations of the longitudinal B_1 and lateral A_1 cyclic pitch commands, defined as outlined above, resembles those of a conventional helicopter, where B_1 compensates for the backward flapping of the rotor at increasing speed, whereas the variation of A_1 depends on the lateral flapping which, at least at low speed, is influenced by the longitudinal inflow distribution.

As a further analysis, limiting performance characteristics of the vehicle are determined on the basis of its dynamical model, by comparing an estimate of the necessary power in the considered flight condition against the maximum available power. In the absence of more detailed information on the actual characteristics of the powerplant, the available power is estimated assuming that it remains

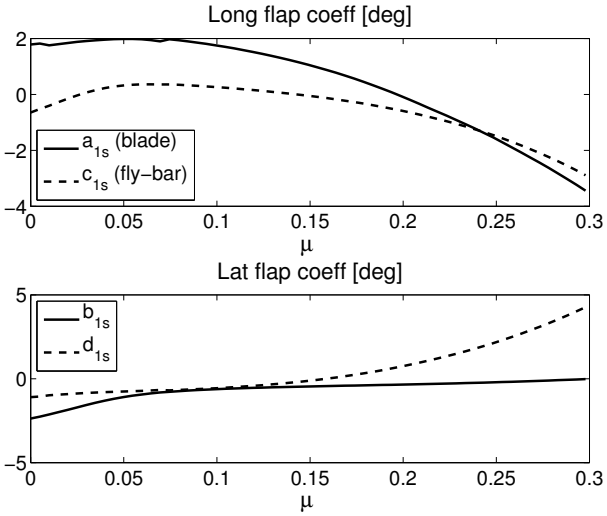

(a) Main rotor flapping coefficients at trim vs. forward speed.

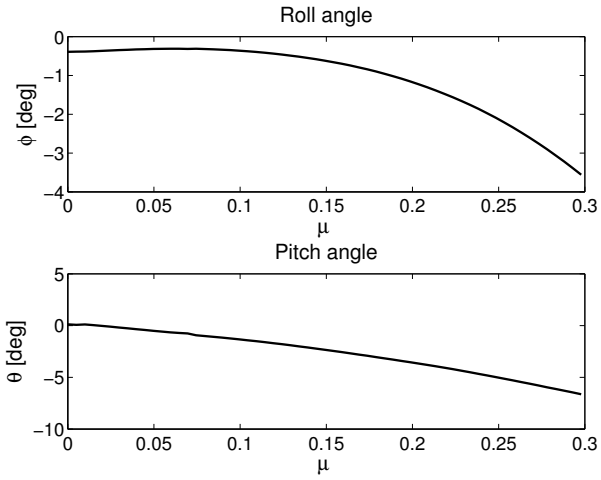

(b) Euler angles at trim vs. forward speed.

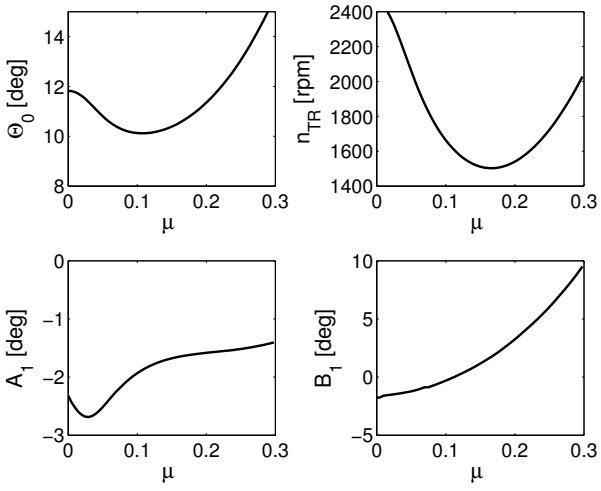

(c) Commands at trim vs. forward speed.

Figure 4: Trim conditions as a function of forward speed

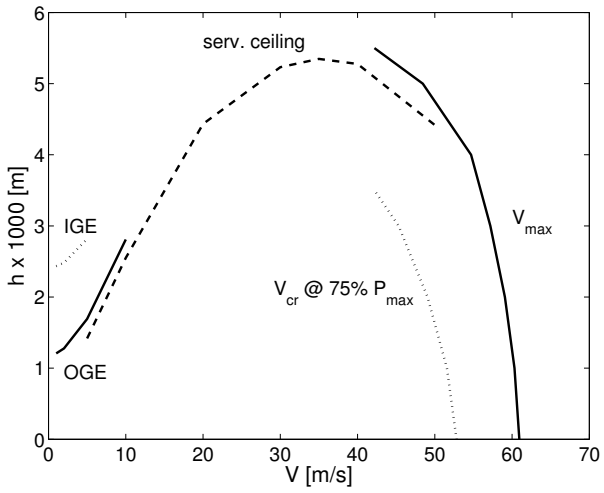

Figure 5: Flight Envelope.

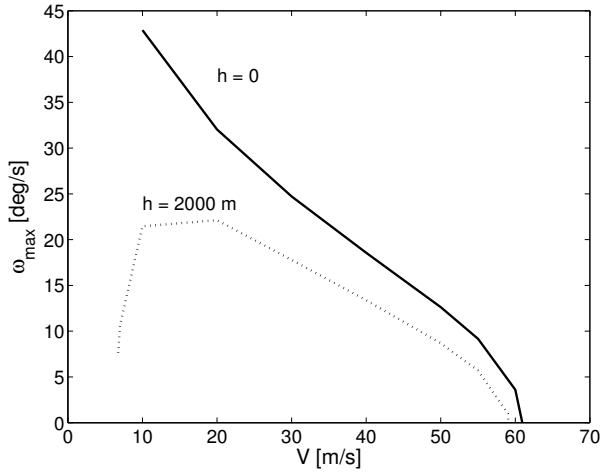

Figure 6: Maximum Turn Rate.

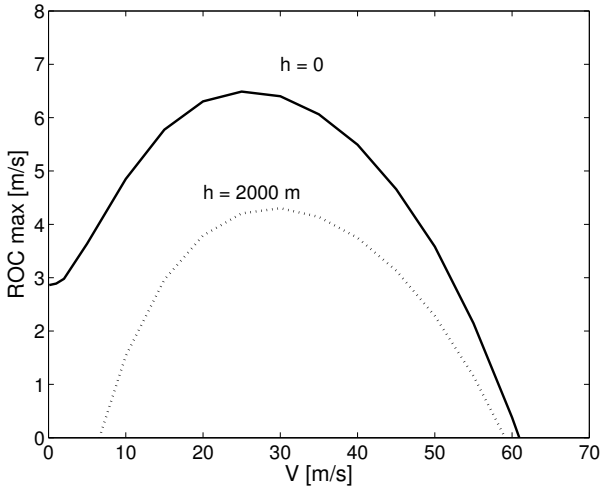

Figure 7: Maximum Rate of Climb.

constant with forward speed (for constant rpm) and proportional to the air density $\rho(h)$, so that it is

$$P_{max}(h) = P_{max,SL}[\rho(h)/\rho_{SL}]^{\sigma}$$

where the subscript SL indicates value at sea level and h is the altitude. The exponent σ, that accounts for the variation of engine performance with the density ratio, is assumed equal to unity. Maximum available power at sea level is $P_{max,SL} = 104$ kW (with both engines operative).

All limiting performance are determined by numerically solving the equation $P_{max}(h) = P_n(V, h, \omega, \dot{h})$, where ω is the turn rate and $\dot{h}$ the rate of climb. As an example, maximum airspeed in level flight at altitude $\bar{h}$ is determined by letting $\omega = \dot{h} = 0$ and evaluating V_{max} such that $P_n(V_{max}, \bar{h}, 0, 0)$ equates the maximum available power. Similarly, service ceiling at a given airspeed $\bar{V}$ is evaluated increasing altitude h until $P_n(\bar{V}, h_{max}, 0, \dot{h}_{SC}) = P_{max}(h)$, with $\dot{h}_{SC}$ equal to 0.76 m/s (150 fpm). Similar conditions can be easily derived for any other limiting performance of interest.

The flight envelope in level flight is shown in Fig. 5 where it appears that service ceiling is above 5000 m at an airspeed of approximately 35 m/s. Maximum airspeed at sea level is approximately 60 m/s. Ceiling in hovering condition out of ground effect is around 1200 m, where this value increases up to more than 2300 m in ground effect.

Maximum turn rate and maximum rate of climb vs. flight speed are reported in Figs. 6 and 7, respectively, at sea–level and 2000 m of altitude. The numerical values obtained for the model are in line with those expected for a vehicle in the VLR weight class.

Stability Analysis

Two different approaches were considered in order to evaluate helicopter stability, with the following objectives: (i) to analyse the effect of the gimballed rotor on stability derivatives of the helicopter; (ii) to interpret the results obtained for the complete helicopter model using models of reduced order with uncoupled dynamics; and (iii) to assess the accuracy of the reduced–order models using the analysis carried out for the the complete model based on the Poincaré mapping technique. The two methodologies can be briefly outlined as follows.

1. Linearization of the quasi-static 6 DoF model [13] allows the rigid-body modes (frequency and damping) to be determined and, among other aspects, the coupling of longitudinal and lateral dynamics to be examined for the purpose of handling qualities evaluation. The linearization of the quasi–static model consists in the numerical evaluation of the elements of the state matrix when each of the state variables $\boldsymbol{x}_B$ of the reduced–order model is perturbed from the steady–state value obtained by the nested trim method. To this end the averaged values (over one

rotor revolution) of the perturbed linear and angular acceleration (and Euler angles rates) are calculated when rotor and inflow states subside, that is, rotor dynamics is assumed faster than helicopter modes (hence the name of the approach).

2. Poincaré map analysis of the complete nonlinear, time–periodic model of the helicopter, that provides information on the stability of the coupled rotor–fuselage system. As a major limitation, this approach does not allow to univocally determine the frequencies of the characteristic modes. For each considered flight condition, the Poincaré map [14] is built starting from the knowledge of the corresponding periodic solution of the states, determined by the shooting method. Such a solution is represented by means of the state vector $\mathbf{p}$ at trim for $\psi = 0$. Point $\mathbf{p}$ is a fixed point for the discrete map that transforms an arbitrary initial state $\mathbf{p} + \delta\boldsymbol{x}$ at $\psi = 0$ into the values of the state variable after an interval $\Delta t = 2\pi/\Omega$. The stability of the periodic solution in the time domain is directly related to the stability of the equilibrium $\mathbf{p}$ for the map. The map is numerically evaluated by perturbing each state variable from the periodic trim condition, and determining the state variables after one period.

The fundamental solution matrix of a particular initial condition, evaluated at a time equal to the period of the orbit, is known as the monodromy matrix which in turn, for a fixed point $\mathbf{p}$, becomes the local linearization of the map evaluated in $\mathbf{p}$. Basically, this means that the monodromy matrix determines the local dynamics of the system at the fixed point that represents the periodic orbit.

The (i,j)–th element of the monodromy matrix $\boldsymbol{DP}|_p$ can be calculated as

$$[\boldsymbol{DP}|_p]_{i,j} = \left[\frac{x_j(\tau) - x_{j_{trim}}}{\Delta x_i(0)}\right]$$

where $x_{j_{trim}}$ is the j$^{\text{th}}$ variable at trim, $x_j(\tau)$ is the j$^{\text{th}}$ variable after one period and $\Delta x_i(0)$ is the perturbation of the i$^{\text{th}}$ variable from its trim condition at $t = 0$.

The stability analysis of the system is then carried out through the analysis of the eigenvalues of $\boldsymbol{DP}|_p$. As for the Floquet analysis [15] the system is unstable if $|\Lambda_j| > 1$ for any eigenvalue of the monodromy matrix.

The eigenvalues $\lambda_j = \sigma_j + i\omega_j$ in the time domain can be obtained from the roots of the map as

$$\lambda_j = \frac{1}{\tau}\ln\Lambda_j \tag{1}$$

where real and imaginary parts of λ are given by

$$\begin{cases} \omega_j = \dfrac{1}{\tau}\arctan(\mathrm{Im}(\Lambda_j)/\mathrm{Re}(\Lambda_j)) \pm n\dfrac{2\pi}{\tau} \\ \sigma_j = \dfrac{1}{2\tau}\log[\mathrm{Re}(\Lambda_j)^2 + \mathrm{Im}(\Lambda_j)^2] \end{cases} \tag{2}$$

Since $\arctan$ is a multivalued function, each frequency may only be determined as a basic frequency plus or minus an integer multiple of $2\pi/\tau$. In this respect it is well known that the correct value of frequency can be identified on the basis of physical reasoning, when in a given condition the frequency of a mode can be determined with no ambiguity. As an example, at hovering the periodically varying terms of the dynamical system have minor effects. As usual, the periodic solution is unstable if $\mathrm{Re}(\lambda_j) > 0$ for any one of the eigenvalues.

Figure 8 shows the eigenvalues of the quasi-static helicopter model at hovering, transformed into the Gauss–plane for the Poincaré map by means of the inverse transformation $\Lambda_j = \exp(\tau\lambda_j)$. These roots are compared with those obtained for reduced–order models obtained uncoupling the longitudinal from lateral–directional dynamics. It is apparent that the roots of the coupled and uncoupled dynamics are similar. Using the eigenvalues of the uncoupled systems to identify the characteristic modes of the rotorcraft [10], we have that the complex conjugate unstable longitudinal and lateral roots correspond, respectively, to the pendulum (phugoid) and dutch-roll modes. The real eigenvalues around $\lambda = -0.3$ are the heave and the spiral subsidences, while the roll and pitch modes are around $\lambda = -1.6$. With the coupled state matrix the roll and pitch subsidences are coupled in a roll/pitch oscillation.

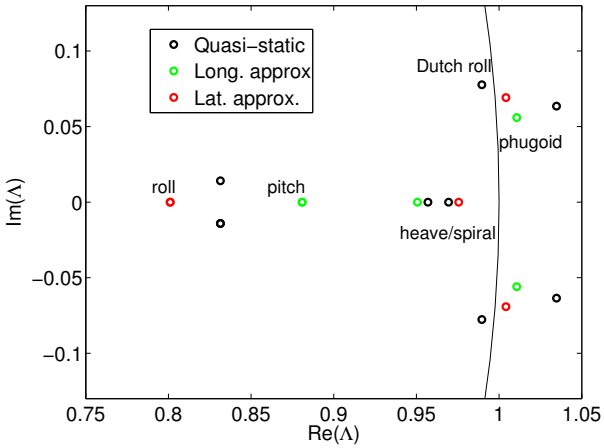

Figure 8: Comparison between eigenvalues of the quasi–static helicopter model and roots for reduced–order decoupled models in hovering.

In Fig. 9 the eigenvalues of the complete helicopter model, calculated by Poincaré map technique, are compared with those of an uncoupled model, where the rigid–body eigenvalues (labeled *Body*) come from the linearization of the quasi–static model, while the Poincaré mapping performed on the isolated rotor provides the eigenvalues labeled *Rotor*. The eigenvalues are plotted as a function of flight speed at sea level, where hovering and maximum speed ($\mu = 0.29$) conditions are identified with a diamond ($\diamond$) and a circle ($\circ$), respectively. The plot demonstrates that the approach based on the analysis of either the isolated rotor or the quasi–static model provides reasonable results when, for the sake of validation, reference is made to the dynamical characteristics of the complete model.

According to the results of the quasi-static model, it

is apparent that the frequencies of the helicopter modes obtained from the eigenvalues of the monodromy matrix (complete model) are in the range $[0,\ \Omega]$. Accordingly, the characteristics of these modes can be studied in the λ-plane using Eqs. (2) with $n = 0$. The same conclusion cannot be drawn for the eigenvalues of the rotor states, as the frequencies are not in the range of the principal values.

Figure 9 shows the eigenvalues of the Poincaré map corresponding to the helicopter (rigid–body) dynamics in forward flight in the Λ-plane (top) together with the eigenvalues of the quasi–static model (bottom). As a general comment some of the characteristic helicopter modes are apparent such as phugoid, short period and dutch-roll, while other modes are in the same frequency range and are difficult to identify. In particular, the roll and pitch modes as well as the heave and spiral (yaw) modes become coupled in certain ranges of flight speed.

The eigenvalues of the quasi-static model (bottom) exhibit an unstable phugoid mode at low and medium speed (see also Fig. 8, where the eigenvalues at hovering are shown). The dutch–roll oscillation is also unstable for velocity lower than $\mu = 0.1$, turning into a stable mode at medium speed. Dutch–roll damping decreases again at high speed, until the mode becomes unstable again for $\mu > 0.28$, whereas mode frequency steadily increases.

The pitch/roll mode uncouples into two subsidences whereas the heave and spiral mode remains stable in the whole range of flight speed. The root locus of the short period mode presents a discontinuity at high speed that depends on the effect of the inflow on the tailplane, as step variations of the stability derivatives (in particular M_w and M_q) result when the tailplane enters and exits the rotor wake.

As for the results of the Poincaré analysis on the complete model, Fig. 10 (top) shows that the dutch-roll mode is stable throughout the speed range and the phugoid is unstable only at very low speed whereas the other eigenvalues present minor variations in comparison with those of the quasi–static model. Apparently, approximating the helicopter modes with the quasi-static model brings to a pessimistic estimate of helicopter stability characteristics.

The eigenvalues of the helicopter characteristic modes computed with the Poincaré technique are shown in Fig. 11 in the λ-plane together with some of the limitations resulting from the requirement on handling qualities for VLR [16]. In particular, the numbers labeled in the figure refer to the following specifications: 1. Any oscillation having a period of less than 5 seconds must damp to $1/2$ amplitude in not more than one cycle, 2. Any oscillation having a period of 5 seconds or more but less than 10 seconds must damp to $1/2$ amplitude in not more than two cycles, 3. Any oscillation having a period of 10 seconds or more but less than 20 seconds must be damped, 4. Any oscillation having a period of 20 seconds or more may not achieve double amplitude in less than 20 seconds, 5. Any aperiodic response may not achieve double amplitude in less than 6 seconds.

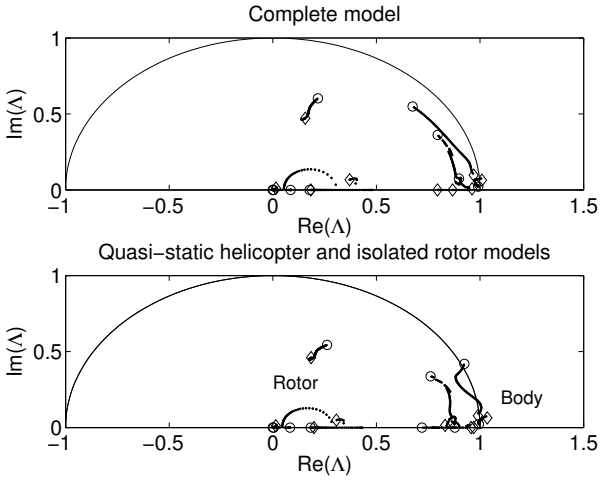

Figure 9: Root loci as a function of speed for linearized Poincaré map of the complete model (top), transformed eigenvalues of the quasi-static model (bottom, Body) and linearized Poincaré map of the isolated rotor (bottom, Rotor)

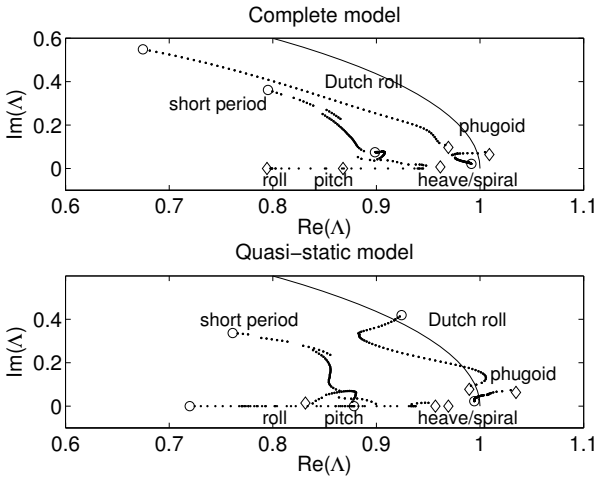

Figure 10: Root loci as a function of speed for rigid–body degrees of freedom of linearized Poincaré map of the complete model (top) and transformed eigenvalues of the quasi-static model (bottom).

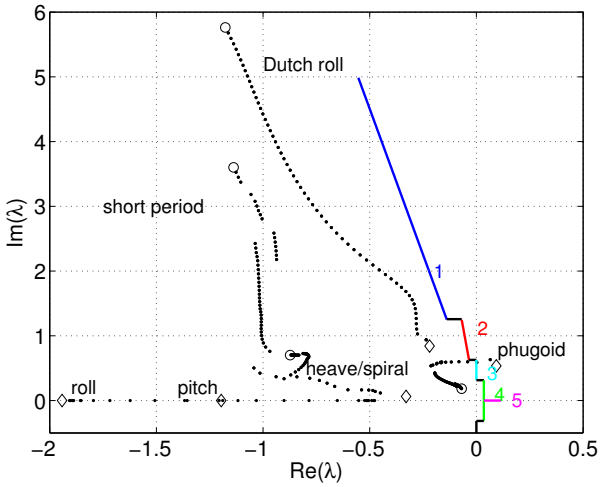

Figure 11: Transformed root locus of rigid–body modes of linearized Poincaré map for the complete model [Eq. (2)], with boundaries of the stability zone defined by CS-27 requirements.

It is apparent from the figure that all the CS–27 requirement are satisfied when the analysis is conducted on the complete model but for the phugoid mode that presents the already observed instability at low speed. It is worth to mention again that when reference is made to the quasi-static model for the sake of comparison, at hovering the phugoid is unstable, with the period between 10 and 20 s, and therefore does not match the requirement 3 whereas at high speed the dutch-roll tends to be marginally stable so that requirement 1 is not satisfied.

Table 1: Main rotor characteristics

Blade			
Radius	R	3.80	m
Chord	c	0.23	m
Teetering mom. of inertia	I_{teet}	176	kg m^2
Built-in coning	β_c	1.8	deg
Undersling	δ	0.06	m
Twist at tip	θ^t_{tw}	-14	deg
Lift slope	a	6.3	
Paddle and fly-bar			
Radius	R_2	1.5	m
Root cut-out	R_1	1.1	m
Chord	c_{fb}	0.25	m
Teetering mom. of inertia	I_{fb}	2	kg m^2
Lift slope	a_{fb}	2.61	
Hub			
Hub stiffness	K	3610	N m/rad
Command ratio	K_H	0.57	
Feathering hinge stiffness	K_{feat}	150	N m/rad

Table 2: Helicopter design parameters.

Fuselage			
Weight	W	7 000	N
Mom. of inertia	I_{xx}	286	kg m^2
	I_{yy}	550	kg m^2
	I_{zz}	630	kg m^2
Equivalent flat plate area	S_{f_x}	0.6	m^2
	S_{f_y}	2.2	m^2
	S_{f_z}	1.3	m^2
Horizontal tail			
Surface	S_h	0.1	m^2
Aspect Ratio	AR_h	1.9	
C_L attenuation factor	k_h	0.6	
Vertical fin			
Surface	S_v	0.4	m^2
Aspect ratio	AR_v	3.1	
C_L attenuation factor	k_v	0.6	
Tail rotor			
Radius	R_{TR}	0.46	m
Number of blades	N_{TR}	5	
Solidity	σ_{TR}	0.17	

Conclusions

A nonlinear model of a novel light helicopter featuring a two–bladed, gimbaled rotor was formulated and analyzed in detail. A periodic trim procedure was adopted for the analysis of trim conditions. The stability analysis was conducted using two methodologies, that is, the quasi–static approach, where the steady–states are determined by a nested trim technique, to determine the rigid–body, characteristic modes of the rotorcraft, and the Poincaré mapping method to analyze the stability of the complete model so as to assess the effects of coupling between rotor, inflow and rigid body dynamics.

For what concerns the steady–state analysis, the variation of trim parameters with tip speed ratio was determined and discussed while the performance analysis led to the evaluation of the flight envelope together with turning and climbing flight characteristics. As for the interpretation of trim conditions, when reference is made to the effects of the hub stiffness and in–plane moment due to the engine torque on the gimbaled rotor, the forward tilt of the TPP gives a relevant contribution to the roll moment which, in turn, affects lateral cyclic pitch command and the lateral attitude of the helicopter.

The major conclusions of the stability analysis are as follows

- the quasi–static analysis gives an approximation of the frequencies and dampings of the helicopter characteristic modes, the accuracy of which deteriorates as the amplitude of the wobbling increases. Therefore, the use of this methodology is to be carefully assessed for the purpose of evaluating the flying qualities of the vehicle
- the quasi–static analysis provides valuable information for the interpretation results obtained by the Poincaré mapping technique
- the eigenvalues obtained from the linearized Poincaré map of the complete helicopter can be evaluated with respect to the requirements of the certification specifications. For the considered configuration it appears that the stability of the phugoid mode in hovering and at very low speed is to be improved.

References

1. Lucertini, F.F. "Stability and Flying Qualities of a Light Helicopter", Ph.D. Thesis, Department of Mechanics and Aeronautics, University of Rome "Sapienza", Rome, June 2010.
2. Avanzini, G., De Matteis, G., Lucertini F.F., and Torasso A., "Dynamic Behaviour and Response of a Two-Bladed Gimballed Rotor." Proceedings of the 36th European Rotorcraft Forum 2010, Paris, September 2010.
3. Peters, D.A., Izadpanah, A.P., "Helicopter trim by periodic shooting with Newton-Raphson iteration", American Helicopter Society, 37th Annual Forum, Vol. 17, New Orleans, LA, May 1981.

4. McVicar, J.S.G., Bradley, R.,"Robust and efficient trimming algorithm for application to advanced mathematical models of rotorcraft", Journal of Aircraft, Vol. 32, No. 2, 1995, pp. 439–442.

5. Avanzini, G., De Matteis, G., and Torasso, A., "Comparison of Helicopter Trim Techniques," Proc. of the XX Conference of the Italian Association of Aeronautics and Astronautics (AIDAA), Milan, June 29 – July 3, 2009.

6. Chaplin, H.R., "Some Dynamic Properties of a Rigid Two–Bladed Fully Gimballed Tip–Jet Helicopter Rotor with Circulation Control", TM–16–80/16, David W. Taylor Naval Ship Research and Development Center, Bethesdo (MD), August 1980.

7. Chaplin, H.R., "Some Dynamic Properties of a Rigid Two–Bladed Fully Gimballed Rotor with Teetering Feedback", TM–16–86/02, David W. Taylor Naval Ship Research and Development Center, Bethesdo (MD), USA, July 1986.

8. Peters, D.A., HaQuang, N.,"Dynamic inflow for practical applications", Journal of American Helicopter Society, Vol. 33, No. 4, 1988, pp. 64–68.

9. Gavrilets, V., Mettler, B., Feron, E.,"Nonlinear model for a small-size acrobatic helicopter", AIAA Guidance, Navigation and Control Conference, Montreal, Canada, August 2001.

10. Padfield, G.D.,"Helicopter Flight Dynamics: The Theory and Application of Flying Qualities and Simulation Modeling", AIAA Education Series, Washington DC, 1996.

11. Heffley, R.K., Mnich, M.A., "Minimum Complexity Helicopter Simulation Math Model", NASA Technical Report CR-177476, Moffett Field, CA, April 1988.

12. Prouty, R.W., *Helicopter Performance, Stability and Control*, Krieger Publishing Company, Malabar, FL, 2002.

13. Hansen, R.S., "Toward a better understanding of helicopter stability derivatives", NASA Technical Memorandum TM-84277, Moffett Field, CA, August 1982.

14. Guckenheimer, J., Holmes, P., "Nonlinear oscillations, dynamical systems and bifurcation of vector fields", Springer, New York, 1990.

15. Biggers, J.C., "Some approximations to the flapping stability of helicopter rotors", in *Rotorcraft Dynamics*, NASA SP-352, NASA, Washington, DC, 1974.

16. EASA - European Aviation Safety Agency, *Certification Specification for Small Rotorcraft CS–27*, 2003 - last amend 2008.